CHEMISTRY
AN ASIAN JOURNAL

DOI: 10.1002/asia.200800230

Luminescence Resonance Energy Transfer Sensors Based on the Assemblies of Oppositely Charged Lanthanide/Gold Nanoparticles in Aqueous Solution

Jian-Qin Gu, Ling-Dong Sun,* Zheng-Guang Yan, and Chun-Hua Yan*[a]

Abstract: This work demonstrates luminescence resonance energy transfer (LRET) sensors based on lanthanide-doped nanoparticles as donors (D) and gold nanoparticles as acceptors (A), combined through electrostatic interactions between the oppositely charged nanoparticles. Negatively charged lanthanide-doped nanoparticles, YVO_4:Eu and $LaPO_4$:Ce,Tb, with high luminescence quantum yield and good water-solubility, are synthesized through a polymer-assisted hydrothermal method. Positively charged polyhedral and spherical gold nanoparticles exhibit surface plasmon resonance (SPR) bands centered at 623 and 535 nm, respectively. These bands overlap well with the emission of the Eu^{3+} and Tb^{3+} ions within the lanthanide nanoparticles. Herein, the gold nanoparticles are synthesized through a seed-mediated cetyltrimethylammonium bromide (CTAB)-assisted method. The assemblies of the oppositely charged donors and acceptors are developed into LRET-based sensors exhibiting a donor quenching efficiency close to 100%.

Keywords: electrostatic interactions · gold · lanthanides · LRET (luminescence resonance energy transfer) · nanoparticles

Introduction

In the last decade, biosciences, especially the bioanalysis technologies, have switched into high gear with the surging strides of nanoscience and nanotechnology in both theoretical and practical studies, from which numerous interesting "unknown lands" are emerging as prospects for alternative foci for research.[1] Among these is Förster/fluorescence resonance energy transfer (FRET),[2] which is termed luminescence resonance energy transfer (LRET) when lanthanides are involved, since emission lines arise from $4f$–$4f$ transitions, a transition technically termed luminescence to distinguish it from fluorescence.[3] FRET and LRET attract a great deal of attention as powerful techniques in biochemistry and structural biology, possessing the characteristics of near-Angstrom resolution and exquisite sensitivity under physiological conditions.[4] In the FRET process, the efficiency of a dipole–dipole interaction-induced energy transfer can be well evaluated from the distance, spectral overlap, and relative dipole orientations between the donor and acceptor.[5] It is expected that nanomaterials are one of the best choices for the investigation of FRET process,[6] possessing the inherent characteristics for overcoming the limitations of traditional dyes, such as the small Förster critical radii (R_0) values, the uncertainty of the relative dipole orientation, and the photobleaching phenomenon.[7] For example, quantum dots (QDs) are successfully used as donors paired with proximal dyes or gold nanoparticles in biological applications of DNA hybridization analysis,[8] biomolecule inhibition assays,[9] and extracellular matrix metalloproteinase-activity monitoring,[10] because of their broad absorption spectra, size-dependent emission properties, and anti-photobleaching character.[11] However, the blinking behavior of QD limits the measurements at the single-particle level,[12] and the related R_0 value may actually fall within the radius of the QD, resulting in a relatively low FRET efficiency.[10b,13] Compared with QDs, lanthanide-doped nanoparticles also exhibit a significant potential for use as donors in resonance energy transfer.[14] As important phosphors, their emission is different from that of QDs, with the luminescence coming from thousands of individual emission centers in the nanoparticles.[15] In this way, the lanthanide-doped nanoparticles show no emission intermittency, and the energy transfer efficiency is less dependent on the radius of the nanoparticles with many emission centers located at the

[a] Dr. J.-Q. Gu, Prof. Dr. L.-D. Sun, Dr. Z.-G. Yan, Prof. Dr. C.-H. Yan
State Key Lab of Rare Earth Materials and Applications
Peking University
Beijing 100871 (China)
Fax: (+86) 10-62754179
E-mail: sun@pku.edu.cn
yan@pku.edu.cn

Supporting information for this article is available on the WWW under http://dx.doi.org/10.1002/asia.200800230.

surface of the nanoparticles. Furthermore, the lanthanide-doped nanoparticles possess similar unique optical properties to lanthanide chelates, which have been widely utilized in LRET applications.[16] Their high quantum yield and sharp emission peaks result in large R_0 values (about 100 Å). The large Stokes shift and millisecond excited-state lifetime, aiding in the avoidance of direct excitation of acceptors and the distinguishing of auto-fluorescence from the system, ensures a high signal-to-background ratio. Moreover, the unpolarized luminescence ensures the accuracy of the LRET analysis.[3,17] Gold nanoparticles are another kind of nanomaterial used as quencher-type acceptors in the resonance-energy-transfer analysis.[18] With large extinction coefficients around $10^5\ cm^{-1}\,M^{-1}$,[19] gold nanoparticles exhibit an exceptional quenching ability. Furthermore, the extinction spectra, ranging from visible to near-infrared, can be well adjusted through controlling the shape and size of the gold nanoparticles,[20] to ensure significant spectral overlap between the donor emission and the acceptor absorption to facilitate highly efficient energy transfer. The application of gold nanoparticles in resonance-energy-transfer studies also relies strongly on their high monodispersity, good solubility, and high stability against salt-induced aggregation.[19,21] More importantly, a gold nanoparticle has a large surface and an isotropic distribution of dipole vectors to accept energy from the donor, so the gold nanoparticle-based resonance-energy-transfer process is also called nanomaterial surface energy transfer (NSET).[22] The NSET approach is a dipole–dipole interaction-related resonance energy transfer, which is similar to FRET in nature, but is geometrically different. It follows a $1/R^4$ dependence and is capable of measuring distances nearly twice as far as FRET. Furthermore, it is desirable for large-scale measurements, such as nucleoprotein assemblies and conformational changes in DNA duplexes.

Nevertheless, the examples using the size-dependent extinction property of gold nanoparticles to pair with different emission donors are rare, and the application of lanthanide-doped nanoparticles in LRET studies is just in the early stages. In our previous report, the lanthanide-doped nanoparticles can transfer energy to proximal gold nanoparticles through the biotin–avidin affinity, with the emission centers located at/near the surface of the nanoparticles playing a crucial role.[23] Since the energy-transfer process strongly depends on the donor–acceptor distance, it is important to construct well-defined assemblies of lanthanide-doped and gold nanoparticles as a model to investigate the resonance energy transfer between them. Herein, we developed two types of LRET systems. Typical lanthanide-doped luminescent nanoparticles (YVO_4:Eu and $LaPO_4$:Ce,Tb) bind compactly with the respective differently shaped gold nanoparticles, through an electrostatic affinity in aqueous solution. Two kinds of positively charged gold nanoparticles are synthesized through the seed-mediated cetyltrimethylammonium bromide (CTAB)-assisted method,[20c] with extinction peaks centered at 623 and 535 nm. The extinction spectra of gold nanoparticles overlap significantly with the most intense emissions of the negatively charged YVO_4:Eu and $LaPO_4$:Ce,Tb nanoparticles. The electrostatic interaction between the oppositely charged donors and acceptors brings them close to each other, thus, leading to an obvious luminescent quenching. The formation of the donor–acceptor assemblies and the energy-transfer process between them are characterized by steady-state and time-decay photoluminescence analyses. This LRET model is instructive to understand the energy-transfer process and mechanism between lanthanide-doped nanoparticles and gold nanoparticles.

Abstract in Chinese:

本文利用静电相互作用，在水溶液中实现了表面分别带有正、负电荷的金和稀土纳米颗粒(YVO_4:Eu 或 $LaPO_4$:Ce,Tb)的组装，形成了以单个金纳米颗粒为中心、稀土纳米颗粒包围的组装体。由于组装体中稀土纳米颗粒的发射光谱与金纳米颗粒的吸收光谱有较大的重叠，形成了以稀土纳米颗粒为供体、金纳米颗粒为受体的发光共振能量转移体系。采用稳态光谱监测和证明了供、受体间的组装和共振能量转移过程；通过荧光寿命研究，揭示了稀土发光中心与金纳米颗粒间的距离对其能量转移效率的影响。

Results and Discussion

Designing of the Donor–Acceptor Pair

We first took the YVO_4:Eu nanoparticles paired with the polyhedral gold nanoparticles as an example to study the LRET process. The donor of YVO_4:Eu nanoparticles was synthesized directly in water by coprecipitation of a given amount of vanadate and the stoichiometric amount of rare earth ions with a molar ratio of Y^{3+}/Eu^{3+} as 92:8.

Appropriate amounts of phosphorous-containing polyacrylic acid (PCA) are used as a capping agent to provide aqueous dispersibility. The PCA polymer contributes to the great stability of the colloidal solution of the nanoparticles, through the coordination with Y^{3+} and Eu^{3+} ions, and provides not only a well coated hydrophilic shell around the nanoparticles, but also repulsion against aggregation arising from their negatively charged -COO^- groups in a weakly basic solution. As shown in Figure 1a, YVO_4:Eu nanoparticles with an average diameter of approximately 50 nm are well dispersed. The selected area electron diffraction (SAED) patterns (Figure 1b) are consistent with a zircon-type YVO_4, with strong diffraction of (200), (301), and (112) planes, that are in good accordance with X-ray diffraction (XRD) patterns (see Figure S1, Supporting Information).[24] The high-resolution TEM (HRTEM) image of an YVO_4:Eu nanocrystal shown in Figure 1c displays well defined lattice fringes of (200) with 0.35 nm spacing, indicating that the nanocrystal is highly crystallized.

The quantum yield of as-prepared YVO_4:Eu nanoparticles is 54%, measured using rhodamine B as reference.[25] Figure 2a shows the emission spectrum of YVO_4:Eu nanoparticles in aqueous solution. The most intense emission located

CHEMISTRY
AN ASIAN JOURNAL

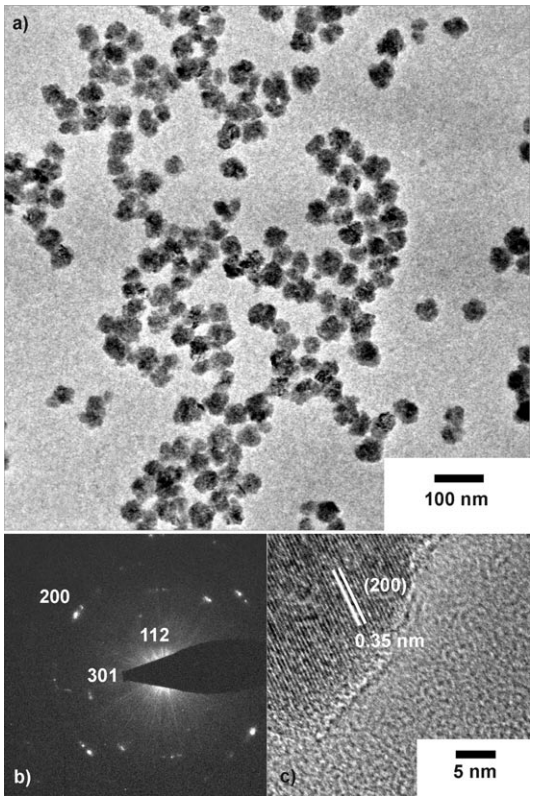

Figure 1. a) Low-resolution TEM, b) selected-area electron diffraction pattern, and c) high-resolution TEM images of YVO_4:Eu nanoparticles.

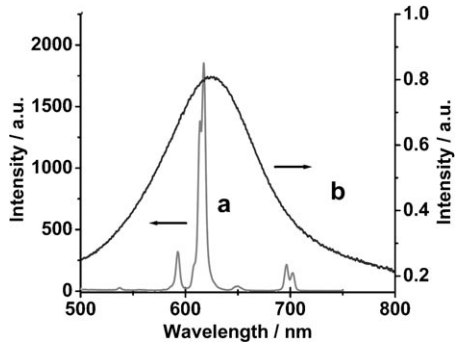

Figure 2. a) Luminescent emission spectrum of YVO_4:Eu nanoparticles; b) UV/Vis extinction spectrum of the as-prepared polyhedral gold nanoparticles.

at 617 nm, with full width at half maximum (FWHM) of approximately 4 nm, comes from the partly released parity-forbidden electric-dipole transition arising from an admixture of odd-parity 5*d*-states into the 4*f* levels ($^5D_0$–$^7F_2$),[26] in which the Förster theory is applicable.[3]

Gold nanopolyhedra serving as the acceptors/quenchers were synthesized through a seed-mediated cetyltrimethylammonium bromide (CTAB)-assisted method.[20c] The as-prepared gold nanopolyhedra are well-dispersed in water and stabilized by the electrostatic repulsion from the positively charged surface with a CTAB bilayer.[27] Figure 3a shows the TEM image of the as-prepared gold nanopolyhedra with

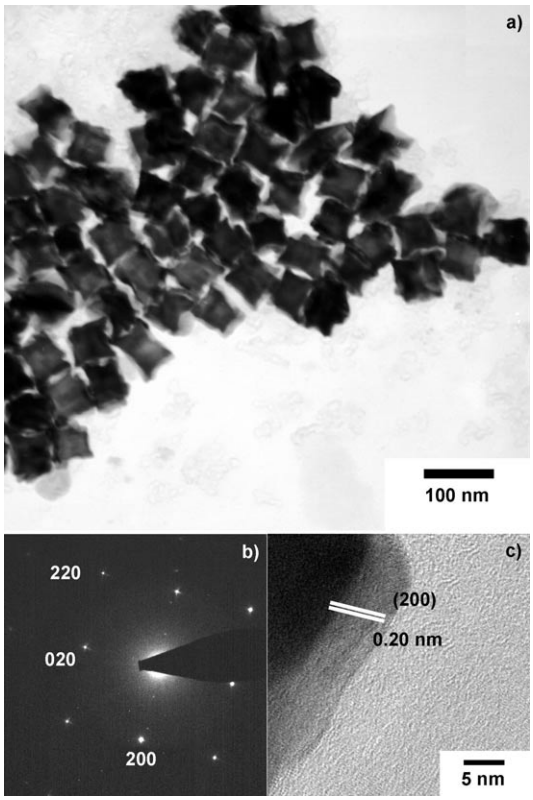

Figure 3. a) Low-resolution TEM, b) selected area electron diffraction pattern, and c) high-resolution TEM images of polyhedral gold nanoparticles.

an average size of approximately 50 nm. The gold nanopolyhedra are homogeneous on a large scale (see SEM image, Figure S2, Supporting Information). According to Figure 3b, SAED patterns attributed to (220), (020), and (200) of a cubic phase can be observed, and are in good agreement with the XRD pattern. The HRTEM image in Figure 3c reveals clear lattice fringes with an interplane distance of 0.20 nm corresponding to the (200) lattice space of metallic gold.[28] Generally, gold nanostructures exhibit strong surface plasmon resonance (SPR) extinction bands, which depend on their shape and size. An extinction band of the as-prepared gold nanopolyhedra, ranging from 500 to 800 nm centered at approximately 623 nm, can be observed in the extinction spectrum (Figure 2b). The peak is symmetrical, further demonstrating the uniformity of the as-prepared gold nanopolyhedra. Thereby, with sufficient spectral overlap between the most intense emission band of YVO_4:Eu nanoparticles and the extinction band of gold nanopolyhedra, effective energy transfer is liable to take place when their spacing is shorter than the critical distance.

LRET Process

Scheme 1 shows the LRET process between YVO_4:Eu and gold nanoparticles. The YVO_4:Eu nanoparticles and gold nanopolyhedra possess oppositely charged surfaces in weakly basic solution. When these two nanoparticles are

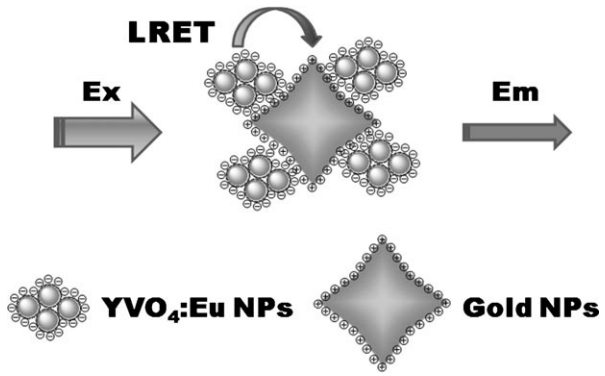

Scheme 1. Schematic illustration of the LRET process from the YVO_4:Eu nanoparticles to polyhedral gold nanoparticles.

mixed together, assemblies are formed with the electrostatic affinity as the driving force, and the particle distances become close enough to trigger an efficient energy transfer from the excited YVO_4:Eu nanoparticles to gold nanopolyhedra. To illustrate the LRET process in detail, the experiment was carried out by gradually adding small amounts of a solution of gold nanopolyhedra to an YVO_4:Eu solution. The content of YVO_4:Eu, which can be evaluated from the total amount of nanoparticles and their sizes, was maintained at 1.6×10^{8} particle cm^{-3} (2.6×10^{-10} mol L^{-1}), while the content of the gold nanopolyhedra acceptor was varied from 2×10^{6} particle cm^{-3} (3.3×10^{-12} mol L^{-1}) to 2×10^{7} particle cm^{-3} (3.3×10^{-11} mol L^{-1}). As shown in Figure 4a, a pronounced and progressive quenching of the donor luminescence is clearly observed as the ratio of gold to YVO_4:Eu is increased, and the luminescent intensity of the donor approximately reaches a minimum when the acceptor/donor ratio gets to 1:8. As mentioned previously, the LRET experiment was carried out in a sufficiently dilute solution to minimize the interference from the absorption of incident light, inner-filter effects such as re-absorption of luminescence, and the aggregation of congeneric nanoparticles. At such low concentrations, the donors and acceptors could be assumed to be noninteracting and isolated in the solution, and so the mean distance between them could be estimated as approximately 2×10^{5} Å from the concentration of nanoparticles, far beyond the distances required for efficient LRET quenching. Therefore, the formation of donor–acceptor assemblies is the prerequisite for our LRET process.

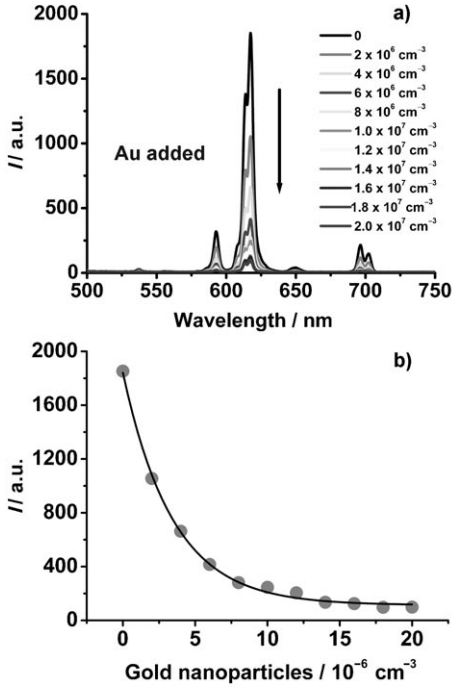

Figure 4. a) Luminescent spectra of the YVO_4:Eu nanoparticles with the addition of gold nanopolyhedra; b) Plot of the apparent luminescent intensity versus the amount of gold nanopolyhedra.

The efficiency of LRET (E_I) is estimated by the equation of $E_I=1-I_{DA}/I_D$, in which I_D and I_{DA} are the intensities of the $^5D_0$–$^7F_2$ transition of Eu^{3+} ions in the YVO_4:Eu nanoparticles without and with LRET assemblies, respectively. The dots in Figure 4b show the luminescence tendency with the addition of gold nanopolyhedra. At the final stage, the luminescent quenching efficiency of YVO_4:Eu reaches a value of 95%, that is, the greater part of the luminescence is quenched through LRET by the gold polyhedra in the assemblies. The residual luminescence, however, should be attributed to transitions with disoriented dipoles or even less efficient resonance energy transfer for the emission centers inside the lanthanide nanoparticles.[23] More interestingly, the black curve in Figure 4b shows the dependence of I and the amount of gold nanopolyhedra, which is well fitted to a single exponential model ($R^2=0.99$, see Supporting Information for additional analysis). Directed by the above analysis, the dynamic process for the formation of donor–acceptor assemblies can be described according to the equation $n\,D+m\,A\leftrightarrow m\,(D_xA)+(n-mx)\,D$, in which n and m are the numbers of donor and acceptor particles in solution, respectively, and x is the average number of donor particles in each assembly. The fitting to an exponential curve expresses the relationship between luminescence intensity and gold concentration. The concentration of gold nanoparticles is much less than what is required in a simple absorption scheme, so the previously mentioned exponential tendency suggests the influence of the number of free luminescent nanoparticles, which is related to the amount of gold nanoparticles in the system. That is, a gold nanoparticle seems to insert into a fixed volume of the lanthanide nanoparticles forming an LRET assembly when it is added to the solution, showing the exchange between assemblies to be important.

The UV/Vis absorption spectrum (Figure 5) and TEM image (inset of Figure 5) of the assemblies further confirm the previous discussion. The band at 272 nm is attributed to the absorption from vanadate groups of YVO_4:Eu nanoparticles,[26b] and the band at 623 nm is attributed to the absorption of the polyhedral gold nanoparticles. Compared with the spectra of free YVO_4:Eu nanoparticles, the invariant peak position, as well as the weak absorption intensity, indicates that the quenching of YVO_4:Eu emission is most likely to be caused by energy transfer from donor to accept-

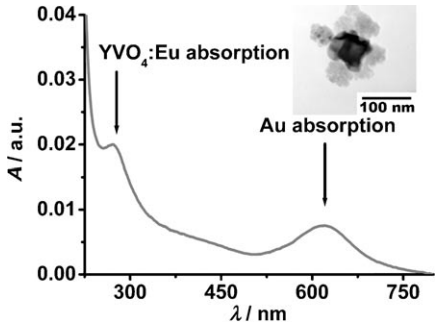

Figure 5. The absorption spectrum of YVO_4:Eu-gold nanopolyhedron assemblies. The inset is a TEM image of the YVO_4:Eu-gold nanopolyhedron assembly.

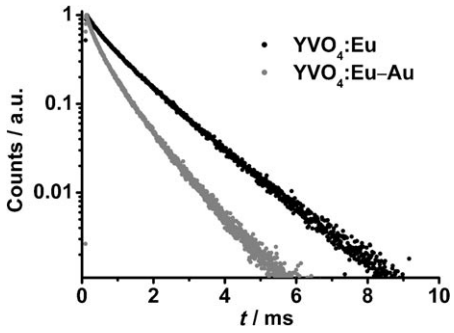

Figure 6. Time decay curves of the free YVO_4:Eu nanoparticles (black), and YVO_4:Eu-gold nanopolyhedron assemblies (gray).

or. Since no spectral shift is observed in the absorption wavelength of gold in assemblies, this shows that the gold nanopolyhedra remain isolated, for the aggregation of gold nanoparticles would alter the SPR bands.[29] Based on the evidence mentioned previously, we suggest that the assemblies are comprised of several YVO_4:Eu donors but one gold acceptor. The TEM image of the assemblies confirms the suggestion, that the assembly shows one gold nanopolyhedron located at the center, enclosed with several YVO_4:Eu nanoparticles. It is inferred that the repulsion of gold nanoparticles might occur because of the assemblies.

It is well-known that the LRET process, which can be recognized as an additional relaxation pathway of the excited states of the donor, should also decrease the lifetime of the excited state.[30] In our previous work, we showed how the analysis of the donor's excited-state lifetimes can also distinguish the contributions of different emission centers.[23] Figure 6 shows the time-decay curves for the $^5D_0$–$^7F_2$ transition of Eu^{3+} ions in YVO_4:Eu nanoparticles with and without the LRET process, and indicates a significant decrease of excited state lifetime after the formation of donor–acceptor assemblies. Both decay curves can be fitted to the equation $y = A_1\exp(-t/\tau_1) + A_2\exp(-t/\tau_2)$, in which τ_1 and τ_2 are the fast and slow excited-state lifetime of the YVO_4:Eu nanoparticles, respectively, and A is the contribution of the two different lifetimes. The fitted results are shown in Table 1. The emission centers at/near the surface of the nanoparticle account for the short excited-state lifetime, since the $^5D_0$–$^7F_2$ transition of Eu^{3+} ions is close to the third harmonic of the OH vibrational mode of water, and therefore releases the energy nonradiatively,[25] whilst the emission centers inside the nanoparticles account for the intrinsic long excited-state lifetimes. Comparatively, in the case of assemblies, both τ_1 and τ_2 are shortened, arising from another nonradiative channel supplied by the neighboring gold nanopolyhedra. The LRET efficiencies can also be determined by the excited-state lifetimes through the equation, $E = 1 - \tau_{DA}/\tau_D$, in which τ_{DA} and τ_D are the luminescent lifetimes of YVO_4:Eu in the presence and absence of the acceptors, respectively. The LRET efficiencies, E, calculated using the short lifetime is 36%, and with the long lifetime is

Table 1. Comparison of the excited-state lifetimes of free YVO_4:Eu nanoparticles and the YVO_4:Eu-gold nanopolyhedron assemblies.

	τ_1[a]/ms	A_1[b]/%	τ_2[a]/ms	A_2[b]/%
YVO_4:Eu	0.58	18.49	1.36	81.51
YVO_4:Eu-Au	0.37	33.76	0.94	66.24

[a] τ_1 and τ_2 are the lifetimes of Eu^{3+} fitting with biexponential function; [b] A_1 and A_2 are the contribution fractions of τ_1 and τ_2, respectively.

31%. These values are much less than the efficiency calculated with the luminescence intensity. Thousands of independent luminescent centers, at which energy is released, transferred, and quenched independently, discrepantly behave like isolated dipole donors in the LRET process, because of the disparate distances between the emission centers and the gold nanopolyhedron surface, and also the sensitive donor/acceptor distance-dependent LRET efficiency. When the Eu^{3+} ions at the surface are concerned, the distances to the gold acceptor are relatively short and the LRET efficiencies are high. On the other hand, for the body-centered Eu^{3+} ions, the large donor/acceptor distance results in a low LRET efficiency. Although the contribution of Eu^{3+} ions inside the nanoparticles to the lifetime is considerable, that of the surface Eu^{3+} ions is minor. In this way, E_τ is less than E_I, but provides additional information about the contributions of different emission centers. Furthermore, gold nanopolyhedra can not only increase the nonradiative decay rate of the donor, but also decrease the radiative rate,[18c,19] thus leading to a high quenching efficiency in the compact donor–acceptor assemblies.

LRET in $LaPO_4$:Ce,Tb Nanoparticle–Gold Nanosphere

The previously mentioned LRET model can also be extended to another important lanthanide phosphor, $LaPO_4$:Ce,Tb nanoparticles as donor, again with gold nanoparticles as acceptor. The $LaPO_4$:Ce,Tb nanoparticles were synthesized through a similar method as the YVO_4:Eu nanoparticles.[23] The surface of the nanoparticles is protected by the PCA polymer, and is also negatively charged. The TEM image (Figure S3a, Supporting Information) indicates that the La-

PO_4:Ce,Tb nanoparticles are quasispherical in shape with an average diameter of about 5 nm.

The luminescent spectrum of $LaPO_4$:Ce,Tb nanoparticles is shown in Figure 7, in which the most intense emission, located at 540 nm, comes from the $^5D_4$–$^7F_5$ transition of Tb^{3+}

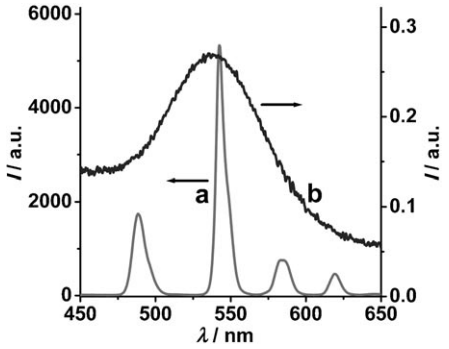

Figure 7. a) Luminescent emission spectrum of $LaPO_4$:Ce,Tb nanoparticles. b) UV/Vis extinction spectrum of spherical gold nanoparticles.

ions. The positively charged acceptor gold nanosphere, with an average diameter of approximately 40 nm (Figure S3b, Supporting Information), was synthesized through the seed-mediated CTAB-assisted method by adjusting the concentration of the reductant, ascorbic acid. The SPR extinction band of the gold nanosphere ranges from 450 to 650 nm, with the main peak at 540 nm (Figure 7b). Comparing the emission of the donor and the absorption of the acceptor, sufficient spectral overlap of the donor emission and acceptor absorption can be observed, satisfying the premise for high-efficiency LRET. When the oppositely charged donor and acceptor are mixed together in a dilute aqueous solution, $LaPO_4$:Ce,Tb–gold nanosphere assemblies are formed. Meanwhile, the photoluminescence of $LaPO_4$:Ce,Tb is significantly quenched by the gold nanospheres (Figure 8). The black curve in Figure 8b shows the luminescent intensities of the $^5D_4$–$^7F_5$ transition of Tb^{3+} ions in the $LaPO_4$:Ce,Tb nanoparticles versus the amount of gold nanospheres for the LRET assemblies, which also fits well to a single exponential model ($R^2 = 0.98$). However, at the final stage, about 90% of the luminescence is quenched by resonance energy transfer. This value is a little lower than that of the YVO_4:Eu–gold nanopolyhedra assemblies. The reason is that the $^5D_4$–$^7F_5$ transition of Tb^{3+} ions consists of both a magnetic dipole transition and the electric dipole transition, and only the latter part contributes to LRET.[3] The $^5D_4$–$^7F_5$ lifetime of $LaPO_4$:Ce,Tb–Au nanosphere assemblies decreases compared with free $LaPO_4$:Ce,Tb samples (Figure 9 and Table 2). The E_τ calculated using τ_1 and τ_2 is 65% and 48%, respectively, which are also smaller than E_I. However, the E_τ values are higher than that of the YVO_4:Eu–gold nanopolyhedrum system, because $LaPO_4$:Ce,Tb nanoparticles are smaller than YVO_4:Eu nanoparticles, hence the emission centers are much closer to the acceptor surface, resulting in the higher E_τ.

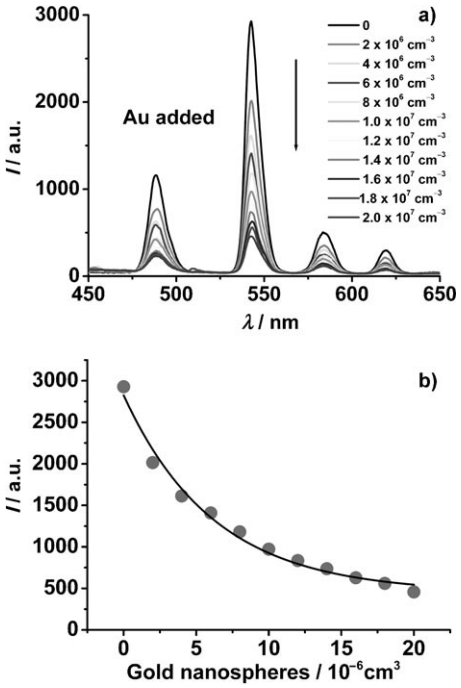

Figure 8. a) Luminescent spectra of the $LaPO_4$:Ce,Tb nanoparticles with the addition of gold nanospheres. b) Plot of the apparent luminescent intensity versus the amount of gold nanospheres.

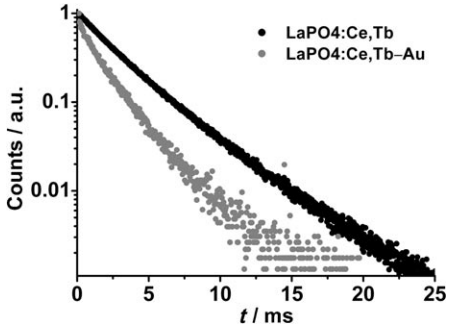

Figure 9. Time decay curves of the free $LaPO_4$:Ce,Tb nanoparticles (black) and $LaPO_4$:Ce,Tb-gold nanosphere assemblies (gray).

Table 2. Comparison of the excited-state lifetimes of $LaPO_4$:Ce,Tb nanoparticles and the $LaPO_4$:Ce,Tb-gold nanosphere assemblies.

	τ_1/ms	A_1/%	τ_2/ms	A_2/%
$LaPO_4$:Ce,Tb	1.87	50.12	3.75	49.88
$LaPO_4$:Ce,Tb-Au	0.65	12.93	2.07	87.07

YVO_4:Eu nanoparticles are also mixed with gold nanospheres to form assemblies, and the energy-transfer efficiency (E_I) is only about 30%. This is reasonable since there is less spectral overlap between the donor emission and acceptor absorption. In our previous report, no LRET occurred between the $LaPO_4$:Ce,Tb and gold nanoparticles with the same charged surface,[23] even with adequate spectra overlap. Therefore, sufficient spectra overlap of the

CHEMISTRY
AN ASIAN JOURNAL

donor and acceptor, as well as a proper donor/acceptor distance, are crucial to an efficient LRET process.

Additionally, electrolytes, which can destroy the electrostatic interaction of the assemblies and accordingly remove the vital conditions for LRET, are introduced to release the luminescence of the lanthanide nanoparticles from LRET assemblies. Upon addition of NaCl (0.1 mol L^{-1}), the luminescent intensity, which diminishes considerably because of the LRET process from the assemblies, recovers as much as 50% of that observed from the free donors, suggesting that this model could be used to detect the strong ions in aqueous solution. Since the distance of donor and acceptor is fixed in this work, we cannot determine the dependence of the LRET efficiency with the donor–acceptor distance. It will be interesting to conduct studies on the interaction distance-dependent resonance energy transfer efficiency between various lanthanide nanoparticles and suited gold nanostructures. It is expected that this kind of donor–acceptor pair will extend LRET studies both experimentally and theoretically to aid LRET investigations to be preferred rather than processes where the efficiency follows a 6th power, like FRET, or 4th power, like NSET.

Conclusions

We present a promising lanthanide-doped nanoparticle to serve as donor with a proximal gold nanoparticle as an acceptor for LRET experiments. The long excited-state lifetime, large Stokes shift, and narrow emissions of lanthanide-doped nanoparticles render LRET analysis particularly straightforward and feasible even in the presence of unbounded acceptors. The SPR bands of gold nanoparticles are adjusted by the shape of the nanoparticles and can be made to overlap with the emission of lanthanide nanoparticles, which leads to highly efficient LRET. Theoretical analysis based on the electrostatic-interaction model of the assembly of oppositely charged nanoparticles fits the experimental data very well. Further studies indicate that the assemblies comprise of several donors with one acceptor, probably caused by differently charged donor and acceptor nanoparticles. Considering the good dispersibility in aqueous solution and easy bio-functionalization, LRET studies based on the lanthanide and gold nanoparticles could be utilised for the measurements of protein–protein, protein–DNA, or oligonucleotide interaction processes. The assemblies could also be used in time-resolved fluorescence assays. The long excited-state lifetimes of lanthanide-doped nanoparticles allow resolved signals, with a high sensitivity, from the analytes to be measured. However, because the size of the donor and acceptors are larger than traditional dyes, the LRET process tends to be influenced by the surface states of the nanoparticles, and the mechanism of LRET between nanoparticles, which is more complicated than that of dyes, requires further clarification.

Experimental Section

Syntheses

YVO_4:Eu and $LaPO_4$:Ce,Tb nanoparticles: Phosphorus-containing polyacrylic acid (PCA), as an aqueous solution and with a phosphorus concentration of 5.85% in weight, was kindly provided by Taihe Chemical Factory in Shandong Province, China. Aqueous solution of the lanthanide nitrates (0.013 mol L^{-1}) was first mixed with a PCA solution (pH adjusted to 6.0), the mixture was stirred for half an hour at room temperature, and then the solution of sodium vanadate (molar ratio of lanthanide ions/sodium vanadate/carboxylate is 1:1:1.5, the doping concentration of europium ions is 8 mol%) were added dropwise. The final pH was adjusted to 12 with a solution of sodium hydroxide (2.5 mol L^{-1}). The mixed solution was transferred into a teflon-lined autoclave and heated at 180 °C for 72 h. Finally, the solution was dialyzed against distilled water to remove the excess ions. A dialysis membrane with a molecular weight cut-off at 12000 Da (pore size of about 2.5 nm) was used, and the water was renewed until the pH value of the colloidal solution was the same as water, and afforded the YVO_4:Eu nanoparticles (0.010 mol L^{-1}). $LaPO_4$:Ce,Tb nanoparticles were synthesized by a similar method by coprecipitation of the lanthanide ions of La^{3+} (40%), Ce^{3+} (45%), and Tb^{3+} (15%) together with Na_2HPO_4.

Polyhedral and spherical gold nanoparticles: A solution of gold seeds (10 mL) was prepared by the reduction of $HAuCl_4{\cdot}3H_2O$ (2.5×10^{-4} mol L^{-1}) by $NaBH_4$ (6.0×10^{-4} mol L^{-1}) in the presence of CTAB (7.5×10^{-2} mol L^{-1}). The solution of $NaBH_4$ was added quickly to the solution containing CTAB and $HAuCl_4$, and the reaction mixture was then shaken for two minutes allowing the escape of the gas formed during the reaction. These seeds were used between 2–24 h after preparation. Gold nanopolyhedra (10 mL) were prepared by mixing $HAuCl_4{\cdot}3H_2O$ (4.0×10^{-4} mol L^{-1}), CTAB (1.6×10^{-2} mol L^{-1}), $AgNO_3$ (6.0×10^{-5} mol L^{-1}), ascorbic acid (1.28×10^{-3} mol L^{-1}), and the as-prepared seed solution (0.5 μL). The solution was mixed by inversion of the test tube after the addition of each component. Gold nanospheres were synthesized using a similar method by changing the ascorbic acid concentration to 4.8×10^{-4} mol L^{-1}.

LRET Experiments

A solution of gold nanopolyhedron (2.5 μL, 4×10^{9} particle cm^{-3}, 6.6×10^{-9} mol L^{-1}) was added in aliquots to a solution of YVO_4:Eu nanoparticles (5 mL, 1.6×10^{8} particle cm^{-3}, 2.6×10^{-10} mol L^{-1}), until the measurements of the emission intensity of YVO_4:Eu remained constant. The LRET process of $LaPO_4$:Ce,Tb to gold nanospheres was carried out by the similar process.

Instrumentation

The size, selected area electron diffraction (SAED), and high-resolution image of the nanoparticles were observed on a JEOL 200CX low-resolution TEM and a Hitachi H-9000 high-resolution TEM (HRTEM), operated at 160 kV and 300 kV, respectively. The samples were prepared by slowly vaporizing a drop of colloidal nanoparticles on carbon-coated copper grids. Absorption spectra were recorded on a Hitachi U-3010 spectrophotometer with colloidal nanoparticles. Luminescent spectra were recorded on a Hitachi F-4500 spectrophotometer equipped with a 150 W Xe-arc lamp at room temperature. The spectra were measured at a fixed band pass of 0.2 nm with the same instrument parameters of 5.0 nm for excitation slit and 5.0 nm for emission slit. The lifetime measurements were performed with an Edinburgh Instruments FLS920 transient/steady-state photoluminescence spectrometer at room temperature.

Acknowledgements

This work is supported by the NSFC (20221101, 20671005, and 20423005), NSFC&RGC (20610068), and the MOST of China (2006CB601104).

[1] a) P. Alivisatos, *Nat. Biotechnol.* **2004**, *22*, 47–52; b) X. Michalet, F. F. Pinaud, L. A. Bentolila, J. M. Tsay, S. Doose, J. J. Li, G. Sundaresan, A. M. Wu, S. S. Gambhir, S. Weiss, *Science* **2005**, *307*, 538–544.
[2] T. Förster in *Modern Quantum Chemistry* (Ed.: O. Sinanoglou), Academic Press, New York, 1965; p. 93.
[3] P. R. Selvin, *IEEE J. Sel. Top. Quantum Electron.* **1996**, *2*, 1077–1087.
[4] a) M. P. Lillo, B. K. Szpikowska, M. T. Mas, J. D. Sutin, J. M. Beechem, *Biochemistry* **1997**, *36*, 11273–11281; b) B. Schuler, E. A. Lipman, W. A. Eaton, *Nature* **2002**, *419*, 743–747; c) X. Zhuang, L. E. Bartley, H. P. Babcock, R. Russell, T. Ha, D. Herschlag, S. Chu, *Science* **2000**, *288*, 2048–2051; d) D. J. Posson, P. Ge, C. Miller, F. Bezanilla, P. R. Selvin, *Nature* **2005**, *436*, 848–851.
[5] a) L. Stryer, *Annu. Rev. Biochem.* **1978**, *47*, 819–846; b) R. H. Faircough, C. R. Cantor, *Methods Enzymol.* **1978**, *48*, 347–379; c) B. Herman, *Methods Cell Biol.* **1989**, *30*, 219–243; d) R. M. Clegg, *Curr. Opin. Biotechnol.* **1995**, *6*, 103–110.
[6] a) E. A. Jares-Erijman, T. M. Jovin, *Nat. Biotechnol.* **2003**, *21*, 1387–1395; b) I. Medintz, A. R. Clapp, H. Mattoussi, E. R. Goldman, B. Fisher, J. M. Mauro, *Nat. Mater.* **2003**, *2*, 630–638; c) B. Dubertret, M. Calame, A. J. Libchaber, *Nat. Biotechnol.* **2001**, *19*, 365–370; d) A. R. Clapp, I. L. Medintz, B. R. Fisher, G. P. Anderson, H. Mattoussi, *J. Am. Chem. Soc.* **2005**, *127*, 1242–1250; e) R. Wargnier, A. V. Baranov, V. G. Maslov, V. Stsiapura, M. Artemyev, M. Pluot, A. Sukhanova, I. Nabiev, *Nano Lett.* **2004**, *4*, 451–457.
[7] a) K. E. Sapsford, L. Berti, I. L. Medintz, *Minerva Biotecnol.* **2005**, *16*, 253–279; b) V. V. Didenko, *Biotechniques* **2001**, *31*, 1106–1121; c) P. R. Selvin, *Biophys. J.* **2003**, *84*, 612–622.
[8] a) H. Peng, L. Zhang, T. H. M. Kjällman, C. Soeller, J. Travas-Sejdic, *J. Am. Chem. Soc.* **2007**, *129*, 3048–3049; b) T. Pons, I. L. Medintz, K. E. Sapsford, S. Higashiya, A. F. Grimes, D. S. English, H. Mattoussi, *Nano Lett.* **2007**, *7*, 3157–3164.
[9] a) E. Oh, M. Y. Hong, D. Lee, S. H. Nam, H. C. Yoon, H. S. Kim, *J. Am. Chem. Soc.* **2005**, *127*, 3270–3271; b) E. R. Goldman, I. L. Medintz, J. L. Whitley, A. Hayhurst, A. R. Clapp, H. T. Uyeda, J. R. Deschamps, M. E. Lassman, H. Mattoussi, *J. Am. Chem. Soc.* **2005**, *127*, 6744–6751.
[10] a) L. Shi, V. D. Paoli, N. Rosenzweig, Z. Rosenzweig, *J. Am. Chem. Soc.* **2006**, *128*, 10378–10379; b) A. R. Clapp, I. L. Medintz, J. M. Mauro, B. R. Fisher, M. G. Bawendi, H. Mattoussi, *J. Am. Chem. Soc.* **2004**, *126*, 301–310.
[11] S. J. Rosenthal, *Nat. Biotechnol.* **2001**, *19*, 621–622.
[12] a) M. Nirmal, B. O. Dabbousi, M. G. Bawendi, J. J. Macklin, J. K. Trautman, T. D. Harris, L. E. Brus, *Nature* **1996**, *383*, 802–804; b) M. Sugisaki, H. W. Ren, K. Nishi, Y. Masumoto, *Phys. Rev. Lett.* **2001**, *86*, 4883–4886; c) S. Weiss, *Nat. Struct. Biol.* **2000**, *7*, 724–729.
[13] I. L. Medintz, J. H. Konnert, A. R. Clapp, I. Stanish, M. E. Twigg, H. Mattoussi, J. M. Mauro, J. R. Deschamps, *Proc. Natl. Acad. Sci. USA* **2004**, *101*, 9612–9617.
[14] a) D. Casanova, D. Giaume, T. Gacoin, J. P. Boilot, A. Alexandrou, *J. Phys. Chem. B* **2006**, *110*, 19264–19270; b) L. Wang, R. Yan, Z. Huo, L. Wang, J. Zeng, J. Bao, X. Wang, Q. Peng, Y. Li, *Angew. Chem.* **2005**, *117*, 6208–6211; *Angew. Chem. Int. Ed.* **2005**, *44*, 6054–6057; c) L. Wang, Y. Li, *Chem. Eur. J.* **2007**, *13*, 4203–4207; d) K. Kuningas, T. Rantanen, T. Ukonaho, T. Lövgren, T. Soukka, *Anal. Chem.* **2005**, *77*, 7348–7355; e) Z. Chen, H. Chen, H. Hu, M. Yu, F. Li, Q. Zhang, Z. Zhou, T. Yi, C. Huang, *J. Am. Chem. Soc.* **2008**, *130*, 3023–3029.
[15] a) A. Huignard, V. Buissette, A. C. Franville, T. Gacoin, J. P. Boilot, *J. Phys. Chem. B* **2003**, *107*, 6753–6759; b) J. W. Stouwdam, F. C. J. M. van Veggel, *Nano Lett.* **2002**, *2*, 733–737; c) H. Meyssamy, K. Riwotzki, A. Kornowski, S. Naused, M. Haase, *Adv. Mater.* **1999**, *11*, 840–844; d) H. X. Mai, Y. W. Zhang, R. Si, Z. G. Yan, L. D. Sun, L. P. You, C. H. Yan, *J. Am. Chem. Soc.* **2006**, *128*, 6426–6436.
[16] a) A. C. Ferrand, D. Imbert, A. S. Chauvin, C. D. B. Vandevyver, J. C. G. Bünzli, *Chem. Eur. J.* **2007**, *13*, 8678–8687; b) L. J. Charbonnière, N. Hildebrandt, R. F. Ziessel, H. G. Löhmannsröben, *J. Am. Chem. Soc.* **2006**, *128*, 12800–12809; c) P. R. Selvin, *Annu. Rev. Biophys. Biomol. Struct.* **2002**, *31*, 275–302; d) A. Tsourkas, M. A. Behlke, Y. Xu, G. Bao, *Anal. Chem.* **2003**, *75*, 3697–3703.
[17] a) K. Kömpe, H. Borchert, J. Storz, A. Lobo, S. Adam, T. Möller, M. Haase, *Angew. Chem.* **2003**, *115*, 5672–5675; *Angew. Chem. Int. Ed.* **2003**, *42*, 5513–5516; b) K. Riwotzki, M. Haase, *J. Phys. Chem. B* **1998**, *102*, 10129–10135; c) M. Tan, G. Wang, X. Hai, Z. Ye, J. Yuan, *J. Mater. Chem.* **2004**, *14*, 2896–2901.
[18] a) D. J. Maxwell, J. R. Taylor, S. Nie, *J. Am. Chem. Soc.* **2002**, *124*, 9606–9612; b) H. Du, M. D. Disney, B. L. Miller, T. D. Krauss, *J. Am. Chem. Soc.* **2003**, *125*, 4012–4013; c) E. Dulkeith, M. Ringler, T. A. Klar, J. Feldmann, *Nano Lett.* **2005**, *5*, 585–589; d) P. C. Ray, A. Fortner, G. K. Darbha, *J. Phys. Chem. B* **2006**, *110*, 20745–20748.
[19] M. C. Daniel, D. Astruc, *Chem. Rev.* **2004**, *104*, 293–346.
[20] a) C. K. Kim, R. R. Kalluru, J. P. Singh, A. Fortner, J. Griffin, G. K. Darbha, P. C. Ray, *Nanotechnology* **2006**, *17*, 3085–3093; b) N. R. Jana, *Small* **2005**, *1*, 875–882; c) T. K. Sau, C. J. Murphy, *J. Am. Chem. Soc.* **2004**, *126*, 8646–8649; d) E. Hutter, J. H. Fendler, *Adv. Mater.* **2004**, *16*, 1685–1706.
[21] a) B. D. Chithrani, W. C. W. Chan, *Nano Lett.* **2007**, *7*, 1542–1550; b) J. W. Stone, P. N. Sisco, E. C. Goldsmith, S. C. Baxter, C. J. Murphy, *Nano Lett.* **2007**, *7*, 116–119.
[22] a) C. S. Yun, A. Javier, T. Jennings, M. Fisher, S. Hira, S. Peterson, B. Hopkins, N. O. Reich, G. F. Strouse, *J. Am. Chem. Soc.* **2005**, *127*, 3115–3119; b) T. L. Jennings, J. C. Schlatterer, M. P. Singh, N. L. Greenbaum, G. F. Strouse, *Nano Lett.* **2006**, *6*, 1318–1324.
[23] J. Q. Gu, J. Shen, L. D. Sun, C. H. Yan, *J. Phys. Chem. C* **2008**, *112*, 6589–6593.
[24] J. A. Baglio, G. Gasurov, *Acta Crystallogr.* **1968**, *24*, 292–293.
[25] A. Huignard, V. Buissette, G. Laurent, T. Gacoin, J. P. Boilot, *Chem. Mater.* **2002**, *14*, 2264–2269.
[26] a) J. C. G. Bünzli, S. Comby, A. S. Chauvin, C. D. B. Vandevyver, *J. Rare Earths* **2007**, *25*, 257–274; b) W. T. Carnall, G. L. Goodman, K. Rajnak, R. S. Rana, *J. Chem. Phys.* **1989**, *90*, 3443–3457; c) C. Brecher, H. Samelson, A. Lempicki, R. Riley, T. Peters, *Phys. Rev.* **1967**, *155*, 178–187.
[27] D. K. Smith, B. A. Korgel, *Langmuir* **2008**, *24*, 644–649.
[28] a) Y. Sun, Y. Xia, *Science* **2002**, *298*, 2176–2179; b) L. Lu, K. Ai, Y. Ozaki, *Langmuir* **2008**, *24*, 1058–1063.
[29] a) M. A. Correa-Duarte, N. Sobal, L. M. Liz-Marzán, M. Giersig, *Adv. Mater.* **2004**, *16*, 2179–2184; b) S. J. Hurst, M. S. Han, A. K. R. Lytton-Jean, C. A. Mirkin, *Anal. Chem.* **2007**, *79*, 7201–7205.
[30] S. Dayal, Y. Lou, A. C. S. Samia, J. C. Berlin, M. E. Kenney, C. Burda, *J. Am. Chem. Soc.* **2006**, *128*, 13974–13975.

Received: June 5, 2008
Published online: August 22, 2008

